Image Cover Sheet

CLASSIFICATION	SYSTEM NUMBER
UNCLASSIFIED	511051

TITLE

Finite Element Analysis of a Broadband Flextensional Transducer

System Number:

Patron Number:

Requester:

Notes:

DSIS Use only:

Deliver to:

Copy No. ___

DEFENCE R&D DÉFENSE

FINITE ELEMENT ANALYSIS OF A BROADBAND FLEXTENSIONAL TRANSDUCER (U)

G.W.McMahon

FanTech Consulting Services

DEFENCE RESEARCH ESTABLISHMENT ÁTLANTIC

Contractor Report

DREA CR 1999-008

January 1999

Défense nationale National Defence

Canada

PLEASE DIRECT ENQUIRIES TO:

THE DIRECTOR GENERAL
DEFENCE RESEARCH ESTABLISHMENT ATLANTIC
P.O. BOX 1012
DARTMOUTH, NOVA SCOTIA, CANADA
B2Y 3Z7

National Defence
Research and Development Branch

Défense nationale
Bureau de recherche et développement

DREA CR 99/008

FINITE ELEMENT ANALYSIS OF A BROADBAND FLEXTENSIONAL TRANSDUCER (U)

G.W.McMahon

FanTech Consulting Service
PO Box 503
Stewiacke, Nova Scotia, Canada
B0N 2J0

Scientific Authority Dennis Jones
D.F.Jones

W7707-8-5999/001/HAL
Contract Number

January 1999

CONTRACTOR REPORT

Prepared for

Defence Research Establishment Atlantic

Centre de Recherches pour la Défense Atlantique

Canada

FINITE ELEMENT ANALYSIS OF A BROADBAND FLEXTENSIONAL TRANSDUCER

ABSTRACT

The Class III flextensional transducer is a dual barrel stave design that shows promise as a broadband projector having a potentially useful bandwidth of over three octaves. A simple axially-symmetric finite element model, for use with the computer modelling program, MAVART, has been set up to aid in the optimization of this design. Performance results predicted by the model are compared with measured results for a DREA experimental Class III barrel-stave projector. The model provides a good representation of the performance, the main discrepancy being in the fundamental resonance frequency, which is 10 % lower than measured. The rubber boot, which was not included in the model, is believed to be the primary reason for the discrepancy. This model will be a useful tool for investigation of changes to the Class III BSP. Greater accuracy is expected with the inclusion of the rubber boot in the model.

RÉSUMÉ

Le transducteur flextensionnel de classe III est un transducteur formé de deux ensembles de douves, prometteur en tant que projecteur à large bande, possédant une largeur de bande potentiellement utile supérieure à trois octaves. Un modèle à éléments finis à symétrie axiale destiné à être utilisé avec le programme de modélisation informatique, MAVART, a été préparé en vue de faciliter l'optimisation de ce transducteur. La performance prévue avec le modèle est comparée aux valeurs mesurées de la performance d'un projecteur expérimental à douves de classe III du CRDA. Le modèle donne une bonne indication de la performance, le principal écart étant observé au niveau de la fréquence de résonance fondamentale, qui est de 10 % inférieure à la fréquence mesurée. La gaine en caoutchouc, dont il n'était pas tenu compte dans le modèle, semblerait être la cause principale de l'écart. Ce modèle constituera un outil commode pour l'étude des changements apportés au projecteur à douves de classe III. On prévoit obtenir une plus grande précision en tenant compte de la gaine de caoutchouc dans le modèle.

CONTRACTOR REPORT

FINITE ELEMENT ANALYSIS OF A BROADBAND FLEXTENSIONAL TRANSDUCER

1. Introduction

Flextensional transducers are characterized by an electromechanical driving mechanism whereby the extensional (compressional) vibration of the driver is transformed into the flexural vibration of an attached shell, generally with substantial mechanical amplification. This produces a large volume velocity in the contiguous acoustic medium for a relatively small motion of the driver. Because these devices are usually small in comparison to the acoustic wavelength at the flexural resonance, the radiation loading is low, resulting in a narrow bandwidth, if high efficiency is to be maintained. A great deal of research has been conducted over the past several years in attempts to increase the bandwidth of flextensional transducers.

Flextensional transducers have been classified into seven classes based on the driver/shell configuration, as described in Reference [1]. Of interest in the present work is the Class III barrel-stave projector (BSP), developed at the Defence Research Establishment Atlantic, in which dual cylindrical drivers vibrating longitudinally excite dual barrel-stave shells in flexural (radial) vibration. The presence of the two shells more than doubles the radiation loading over that of a single-shell BSP (Class I) and, with a longitudinal resonance in the frequency band of interest, a potentially useful bandwidth of over three octaves might be achieved. Reference [2] presents the performance results for an experimental Class III BSP designed and tested at DREA. Two configurations were tested, one with two identical shells and the other with one of the shells machined to a smaller thickness. The performance in terms of bandwidth and source level was promising for both configurations. The aim of the present work is to develop an axially-symmetric finite element model that adequately portrays the experimental results for the first configuration. It can then be used to investigate future improvements in the design by computer modelling, without the need for costly experimentation.

The modelling tool used in the present work is DREA's finite element computer modelling program, MAVART (Model for the Analysis of Vibrations and Acoustic Radiation of Transducers). This program has been used to model Class I BSPs with good agreement with measured performance results [3].

2. Transducer Description

The Class III barrel-stave projector is described in Reference [2]. A cutaway view of the projector is shown in Figure 1. The driver comprises two stacks of 10 axially-poled Navy Type III lead zirconate-titanate rings connected electrically in parallel. Each ring has dimensions: 5.08 cm outside diameter, 5.6 mm wall thickness, and 1.02 cm height. The stacks are bonded to opposite sides of an octagonal steel centre-plate, 2.54 cm thick and 7.24 cm between flats. Octagonal steel end plates 1.57 cm thick are bonded to the other end of each stack.

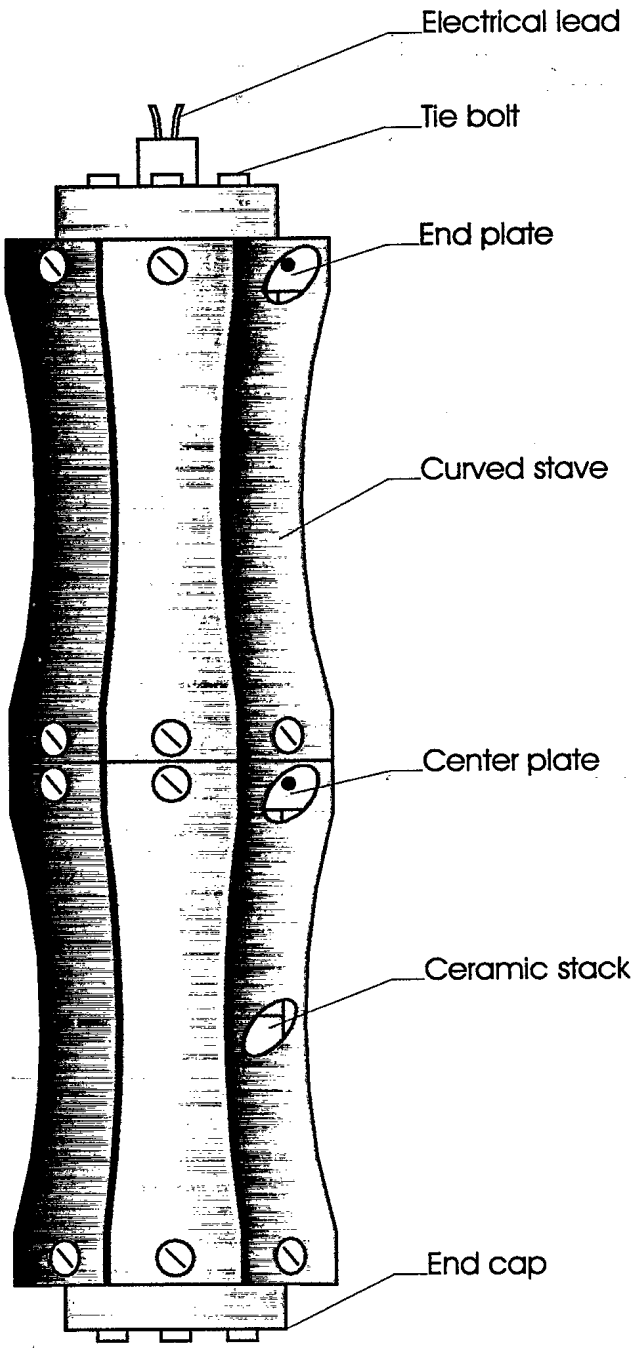

Figure 1 - Class III barrel-stave flextensional projector (rubber boot not shown).

All three steel plates have a central hole 1.1 cm in radius. Aluminum end-caps covering these holes provide support for the electrical leads and four stainless steel tie bolts, which provide axial pre-stressing for the driver. Sixteen identical curved aluminum staves are bonded and bolted to the flat edges of the steel plates, eight on each side of the centre-plate. Each stave is 12.7 cm long with a curved portion 10.2 cm long and 20 cm radius-of-curvature. The mean stave thickness is 4.27 mm. Hence, the stave section has an octagonal inner profile and a circular outer profile. The staves are separated from each other by a 1-mm gap. A 1-mm thick neoprene boot is stretched over the stave section and bonded to the end-plates to seal the gaps against water ingress.

3. Finite Element Modelling

MAVART is an axially-symmetric (2D) modelling tool, so some of the BSP components can be modelled only approximately, in particular the critical stave sections. The stave sections have been modelled as homogeneous circular shells having the same average thickness as the actual staves. The material properties in the axial and radial directions are those of 7075 aluminum reduced by the fraction removed in the gaps, about 3.5%. In the tangential direction, the modulus is softened by a further factor of 500, with a Poisson's ratio of 0.001. The following material properties have been used for the stave sections:

$\rho = 2706.\ kg/m^3$, $Y_{z,r} = 7.15e10\ Pa$, $\sigma_{z,r} = 0.3$,
$Y_\phi = 14.e6\ Pa$, $\sigma_\phi = .001$, $G_\phi = 2.5e10\ Pa$

where ρ is density, Y and G are Young's modulus and shear modulus, respectively, σ is Poisson's ratio, and the subscripts denote the applicable radial-coordinate directions.

The octagonal steel pieces are modelled as circular pieces of the same area, with handbook values for the material properties. Also, handbook values for 6061 aluminum are used for the end-cap properties. The neoprene boot, tie bolts, and electrical leads were not included in the model.

The driver material is Navy Type III lead zirconate-titanate ceramic. Measured resonance and capacitance data for the stacks alone were obtained from DREA, allowing computation of the axial compliance modulus s_{33}^E, the axial piezoelectric strain constant d_{33}, and the dielectric permittivity ε_{33}^T. Book values were used for the other material properties, as they will have little effect on the performance. The full set of property values used is:

$\rho = 7500\ kg/m^3$, $\varepsilon_{33}^T/\varepsilon_0 = 1007$, $\varepsilon_{11}^T/\varepsilon_0 = 1200$,
$s_{11}^E = 10.1e{-}12$, $s_{13}^E = -3.4e{-}12$, $s_{13}^E = -4.8e{-}12$, $s_{33}^E = 15.75e{-}12$, $s_{44}^E = 39.0e{-}12$
$d_{31} = -95e{-}12$, $d_{33} = 225.e{-}12$, $d_{15} = 330.e{-}12$ *

The only other material in the model is sea water for which book property values have been used.

* Symbology used here conforms to the IEEE Standard on Piezoelectricity, ANSI/IEEE Std 176-1978.

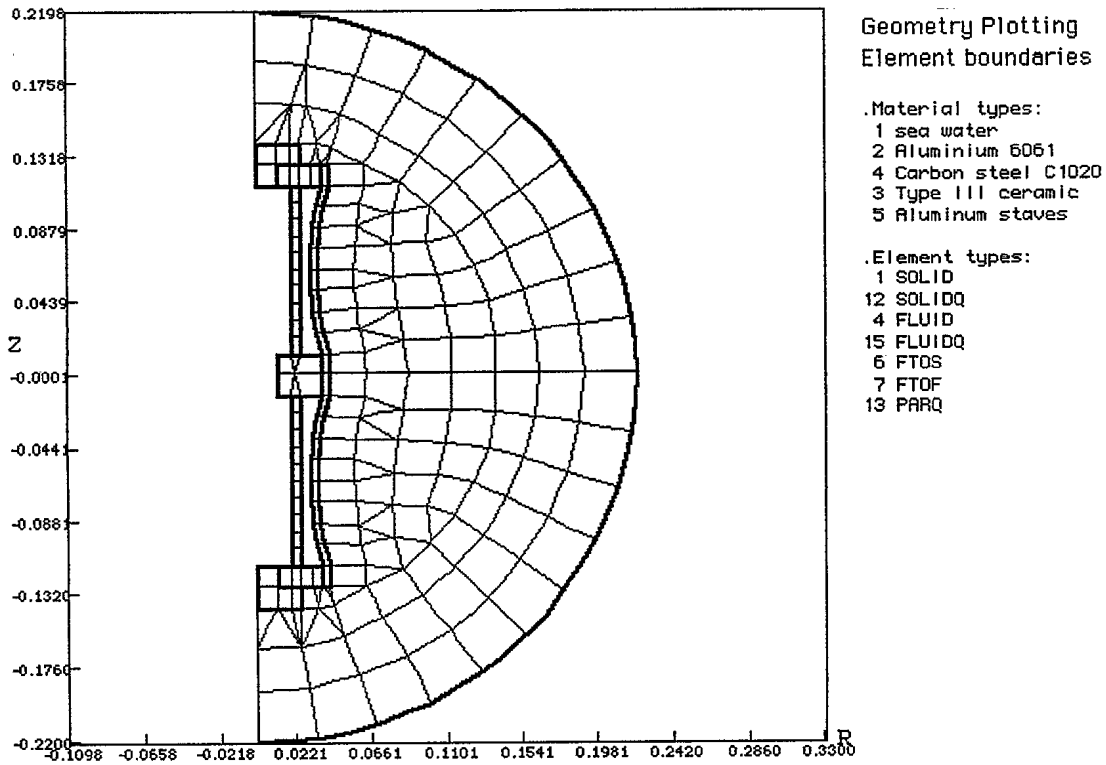

Figure 2 - Finite-element mesh for the full-sphere MAVART model of the Class III barrel stave projector. The material types and MAVART element types are listed on the right of the graph. The projector model itself comprises the components with bold outlines on the left-centre of the mesh, described in more detail in Figure 3. The remainder of the mesh is a sphere of fluid enclosing the projector consisting of triangular FLUID and quadrilateral FLUIDQ elements. The outer boundary of the fluid sphere comprises fluid-to-fluid (FTOF) elements.

A finite element model suitable for analysis by MAVART has been set up with the mesh shown in Figure 2. It has 263 elements, 916 nodes, and 1393 complex degrees-of-freedom (2786 total). As MAVART was configured to handle only 2500 DOF, it was necessary to recompile MAVART for larger array sizes in order to analyze this model in the complex drive mode.

The finite-element mesh for static analysis is prepared by stripping all fluid and fluid-to-fluid elements from the model, leaving only a layer of fluid-to-solid (FTOS) elements on the outer surface of the transducer. Static pressure can then be applied to the nodes in the FTOS elements to simulate immersion depth. The mesh for this model is shown in Figure 3.

For modal analysis, all fluid nodes are removed from the model. Resonance frequencies have been obtained in an eigenvalue analysis with the driver elements shorted. To obtain antiresonance frequencies, the driver elements are connected in parallel and open-circuited.

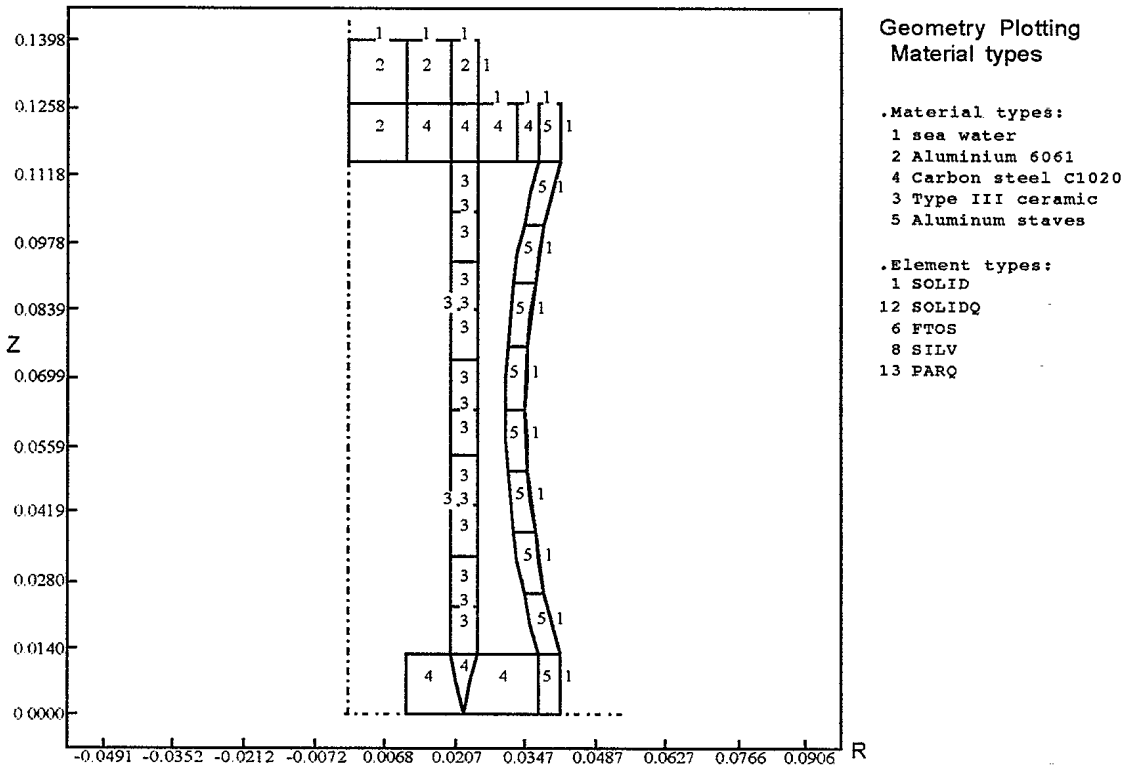

Figure 3 - Finite-element mesh for the upper half of the transducer shown in Figure 2, with the fluid and fluid-to-fluid elements removed. Again the material types and MAVART element types are listed on the right of the graph. Elements are labelled with the appropriate material number. The fluid-to-solid (FTOS) elements comprise a layer of fluid nodes on the outer surface of the transducer. The conductive SILV elements have the same material type as the piezoelectric solid (PARQ). The Z=0 and R=0 axes are indicated by dashed lines.

4. Measured Data

Measured data were obtained from DREA for the experimental Class III BSP. Admittance data on the unbooted projector in air were provided, from which resonance and antiresonance frequencies were extracted. Admittance, transmitting voltage response (TVR), and directivity patterns were provided for the transducer in seawater at an immersion depth of 15 m. Resonance frequency results are summarized below. The resolution of the admittance plots did not allow extraction of the antiresonance for any but the first flexural mode.

Mode 1 (first flexural resonance in air)	2671 Hz
Mode 1 (first flexural antiresonance in air)	2840 Hz
Mode 2 (second flexural resonance in air)	≈5550 Hz
Mode 3 (first longitudinal resonance in air)	6000 Hz
Mode 1 (first flexural resonance in sea water)	1362 Hz
Mode 2 (second flexural resonance in sea water)	≈3500 Hz
Mode 3 (first longitudinal resonance in sea water)	5387 Hz

A very weak resonance was observed on the admittance plot at about 7 kHz for the transducer in air. No other resonances were seen below 14 kHz.

The measured capacitance of the booted transducer in air is 12.46 nF. Other measured data will be displayed later in this report when comparisons are made with the finite element model results.

5. Analysis Procedure and Results

This work deals only with the Class III BSP that has two identical shells. Therefore a plane of symmetry can be applied in the model at z=0, allowing the analysis to be carried out on only half of the structure (i.e., a MAVART half-sphere problem). A trial run on the full sphere model gave essentially identical results to those for the half sphere model, so, to simplify the implementation of changes, the half model has been used in the following.

(a) Modal Analysis

Only four resonances were found by MAVART below 12 kHz. They have been identified as corresponding to the three modes listed above, plus a third flexural resonance, which is very weakly coupled to the piezoelectric driver. The resonance frequencies were found by placing zero voltage fixities to all nodes on the electrode surfaces of the driver. The antiresonance frequencies were found by placing zero voltage fixities to the nodes on the "low" electrodes and connecting the nodes on the "high" electrodes together but leaving them free. The results of the modal analyses are given in Table 1, with the measured results shown for comparison.

Table 1 - Modal Analysis Results

Mode #	Identification	Resonance f_r	Antiresonance f_a	Coupling factor, k_{eff}
MAVART results				
1	First flexural mode	2674.8	2859.1	0.352
2	Second flexural mode	5583.5	5630.3	0.129
3	First longitudinal mode	6073.4	6578.8	0.384
4	Third flexural mode	11085.8	11086.0	≈0.0
Measured results				
1	First flexural mode	2671	2840	0.340
2	Second flexural mode	≈5550		
3	First longitudinal mode	6000		

Computed displacement plots for the four modes are shown in Figure 4. Mode 4 is not observed experimentally, which is not surprising in view of the very low coupling factor.

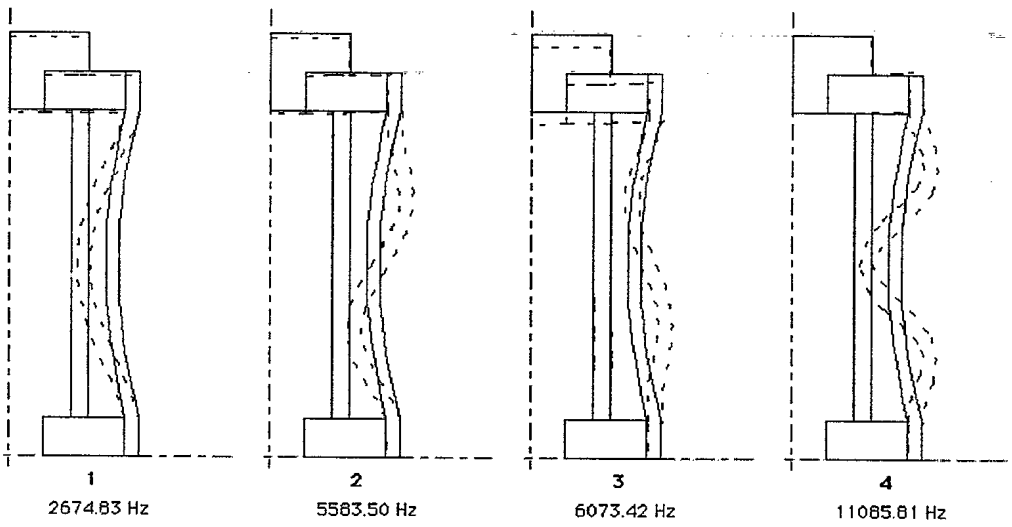

Figure 4 - Computed vibration displacements for the first four resonances obtained in a MAVART modal analysis of the Class III BSP. Only the upper half of the transducer cross section is shown.

(b) Static Analysis

In the static analysis, a pressure fixity of 100 kPa has been applied to each fluid node on the outer surface of the transducer, simulating an immersion depth of about 10 metres. Shown in Figure 5 is a displacement plot of the resulting deformation. Figure 6 displays stress contours in the stave section, where the highest stresses are expected to occur. The R scale is expanded by a factor of three to better resolve the contour lines.

(c) Driven Analyses

A real driven analysis (MAVART CAPAC run) was carried out at 120 Hz, giving a capacitance of 12.1 nF. This is 3% lower than the measured capacitance of 12.46 nF.

A complex driven analysis (MAVART DRIVE run) has been carried out over the frequency band from 500 Hz to 12 kHz. Inertial damping factors of 0.1 and 0.05 have been applied to the stave section and the driver, respectively, to bring the efficiency down to 73% at the fundamental stave resonance, in reasonable agreement with the measured results.

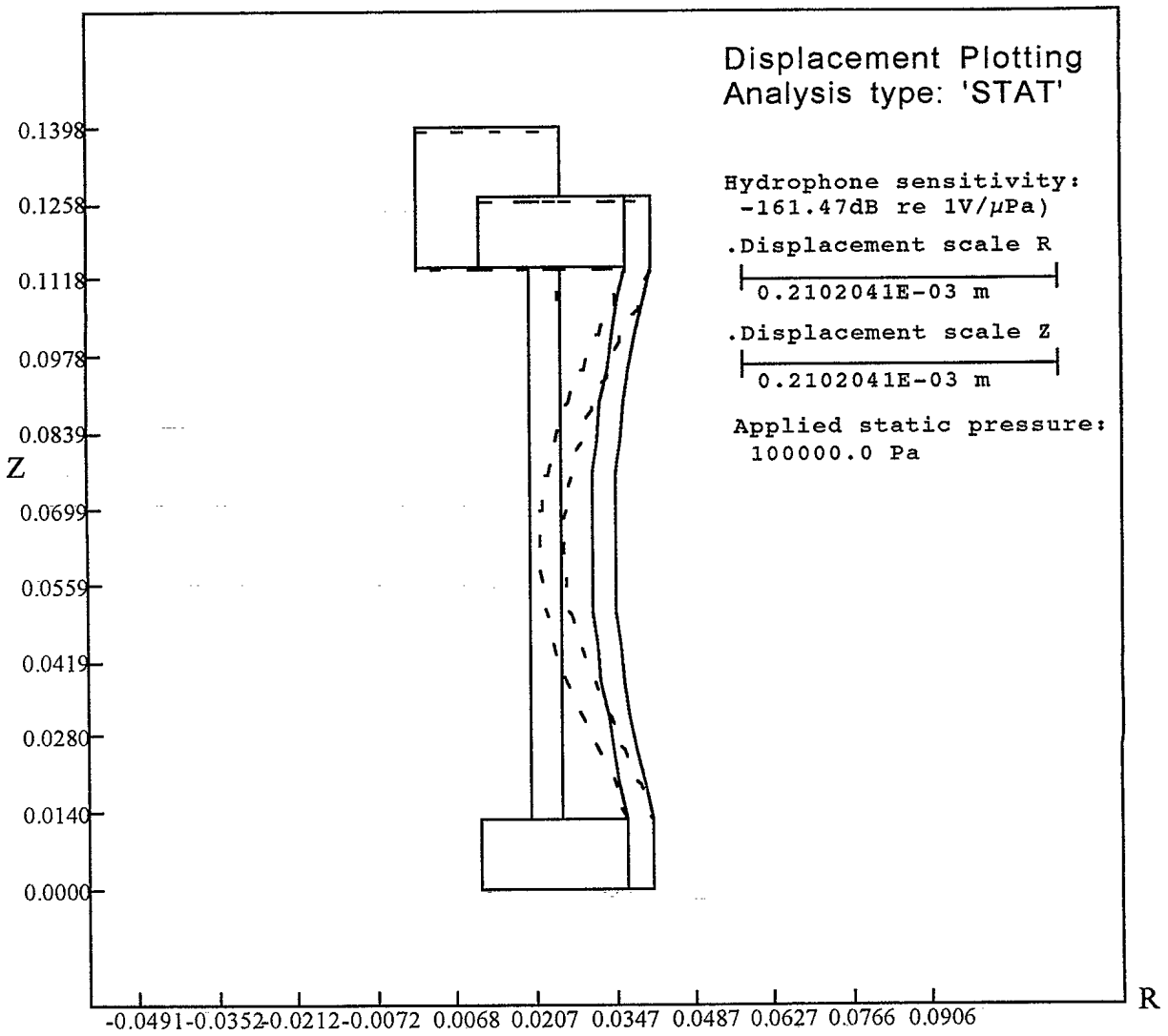

Figure 5 - Computed displacement for an applied hydrostatic pressure of 100 kPa, obtained in a MAVART static analysis of the Class III BSP. Only the upper half of the transducer cross section is shown.

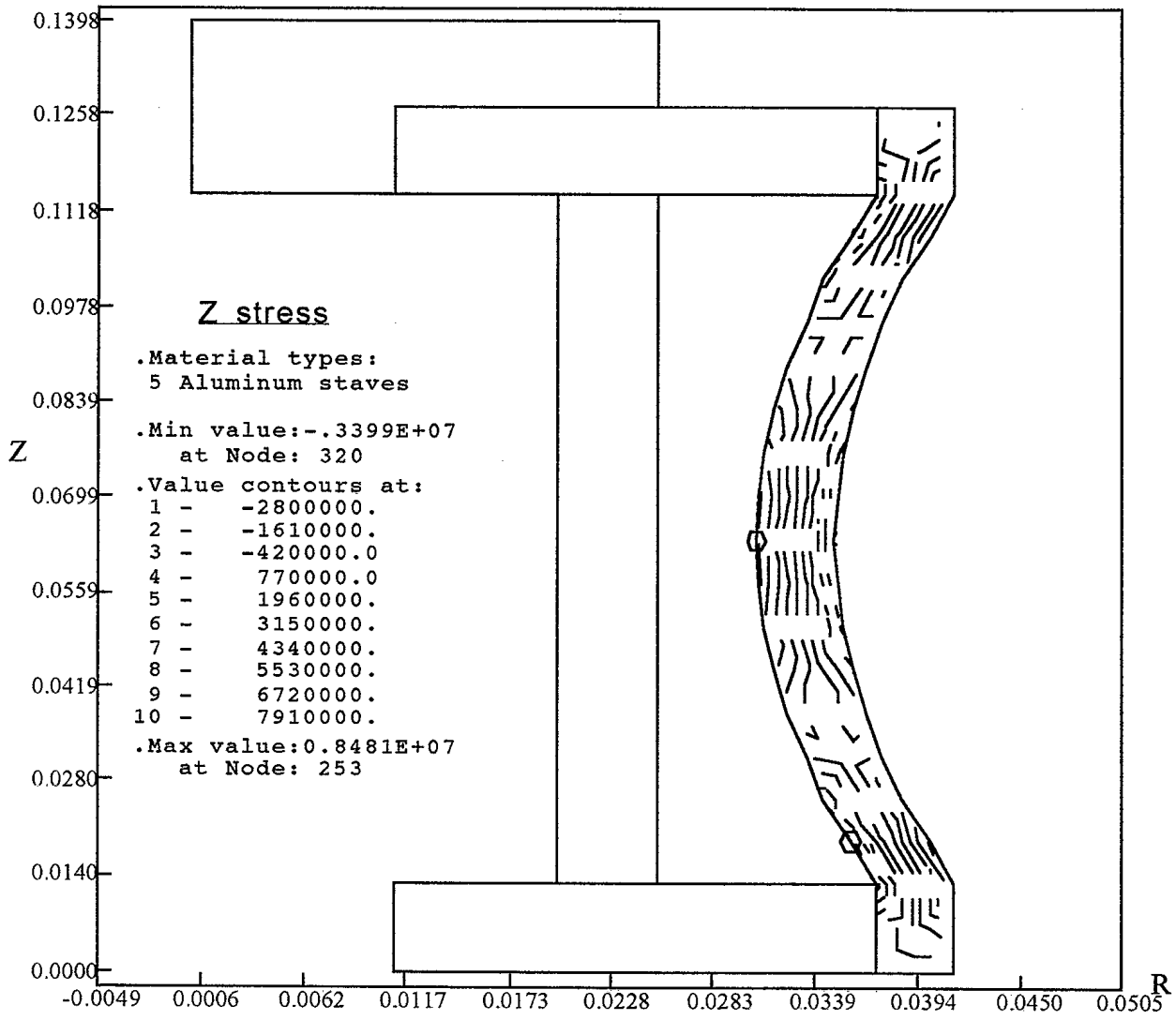

Figure 6 - Computed radial stress contours for an applied hydrostatic pressure of 100 kPa. obtained in a MAVART static analysis of the Class III BSP. Only the upper half of the transducer cross section is shown and the horizontal scale is exaggerated three times to improve the resolution.

Computed and measured transmitting voltage responses (TVRs) are compared in Figure 7 from 500 Hz to 10 kHz. The predicted resonance frequency for the fundamental mode is 1230 Hz, about 10% lower than measured. The predicted peak TVR at the fundamental resonance is 0.8 dB higher than measured. Computed radial and axial TVR curves are plotted in Figure 8 from 500Hz to 10 kHz.

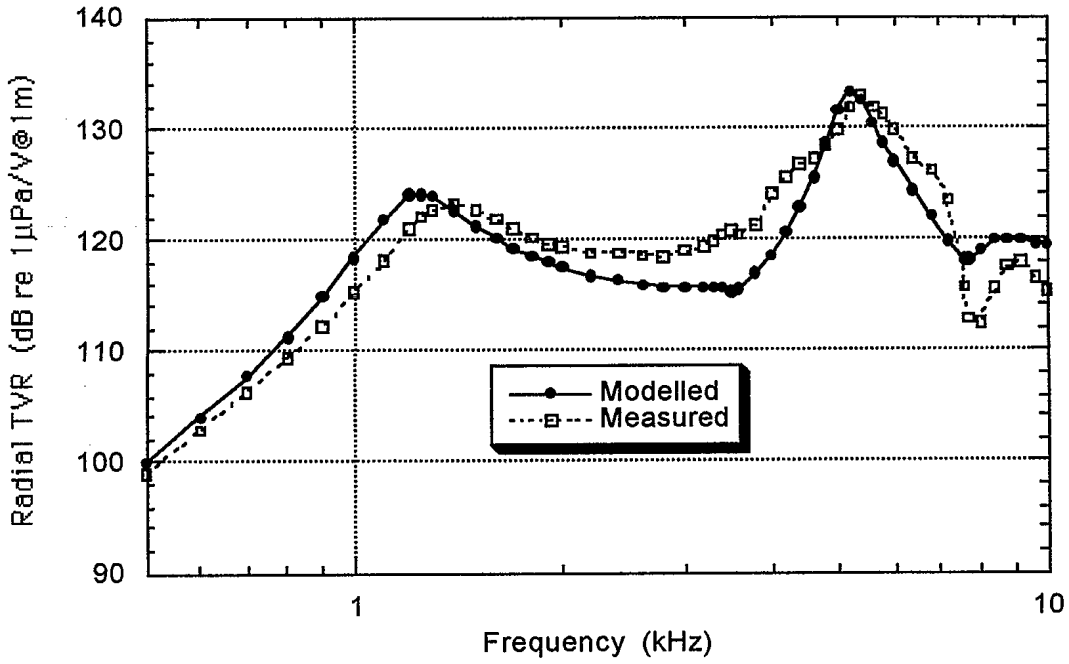

Figure 7 - Comparison of computed and measured radial transmitting voltage response from 500 Hz to 10 kHz for the Class III BSP.

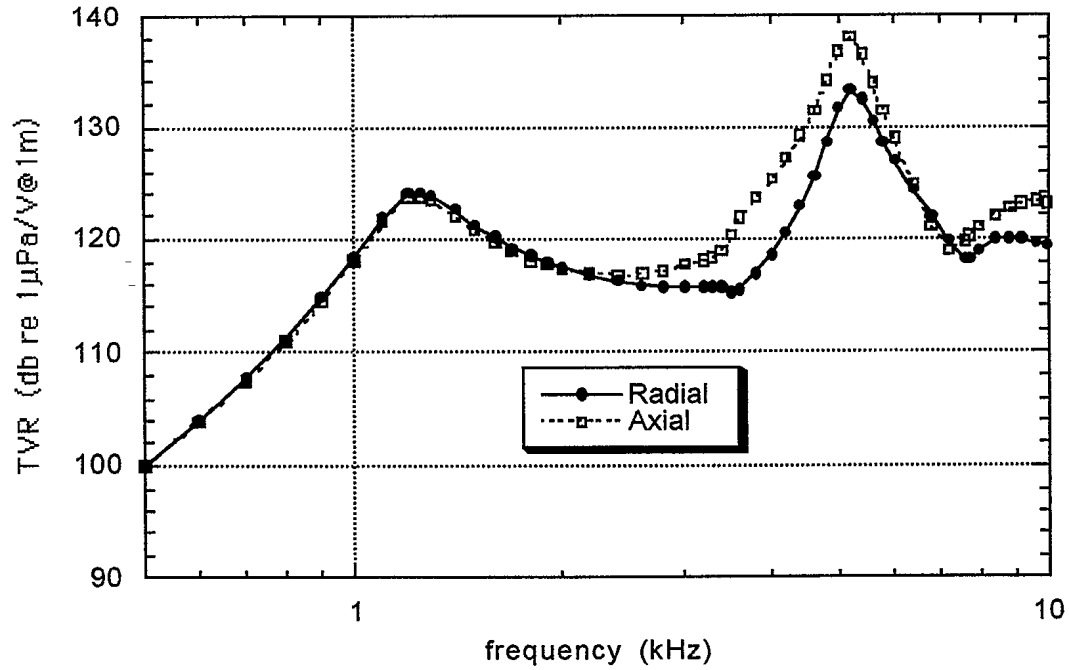

Figure 8 - Computed radial and axial transmitting voltage responses from 500 Hz to 10 kHz for the Class III BSP model.

Figure 9 shows computed admittance curves (conductance and susceptance) for the model over the frequency range from 500 Hz to 10 kHz. Figure 10 shows the same data from 500 Hz to 2kHz, to provide better resolution at the fundamental resonance. Some measured conductance values are plotted for comparison. No measured susceptance values are shown, as they are much higher than computed due to the shunt capacitance of the electrical cable used. Note that the computed conductance is 45% (1.6 dB) higher than measured at the fundamental resonance.

Displacement plots at four drive frequencies are shown in Figure 11. These correspond approximately to the three resonance frequencies seen on the measured TVR curves, and at 7700 Hz, where there is a low point in the radial TVR.

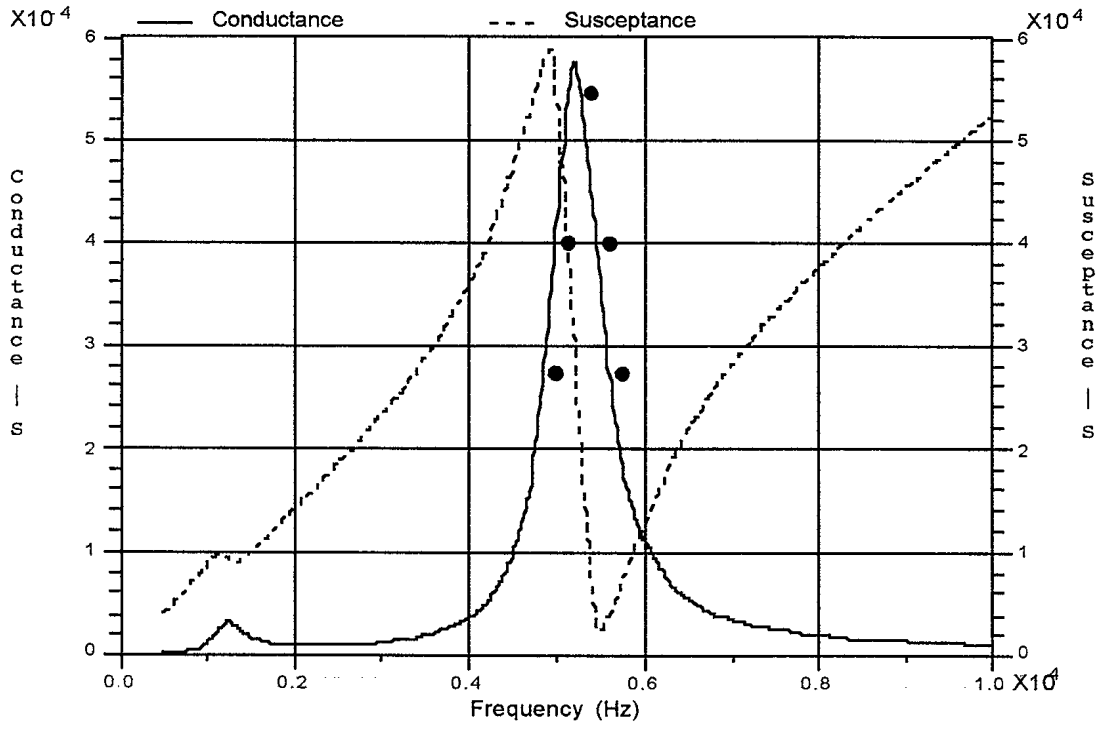

Figure 9 - Computed admittance curves from 500 Hz to 10 kHz for the Class III BSP model. Some measured values of conductance are plotted as solid points.

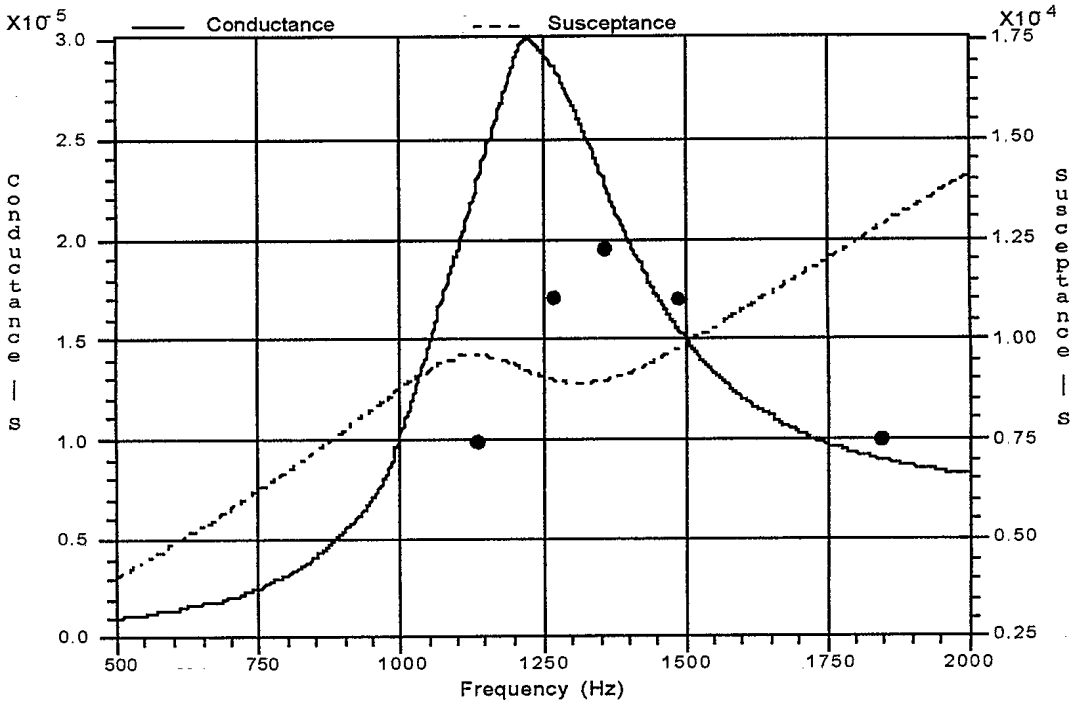

Figure 10 - Computed admittance curves from 500 Hz to 2 kHz for the Class III BSP model. Some measured values of conductance are plotted as solid points.

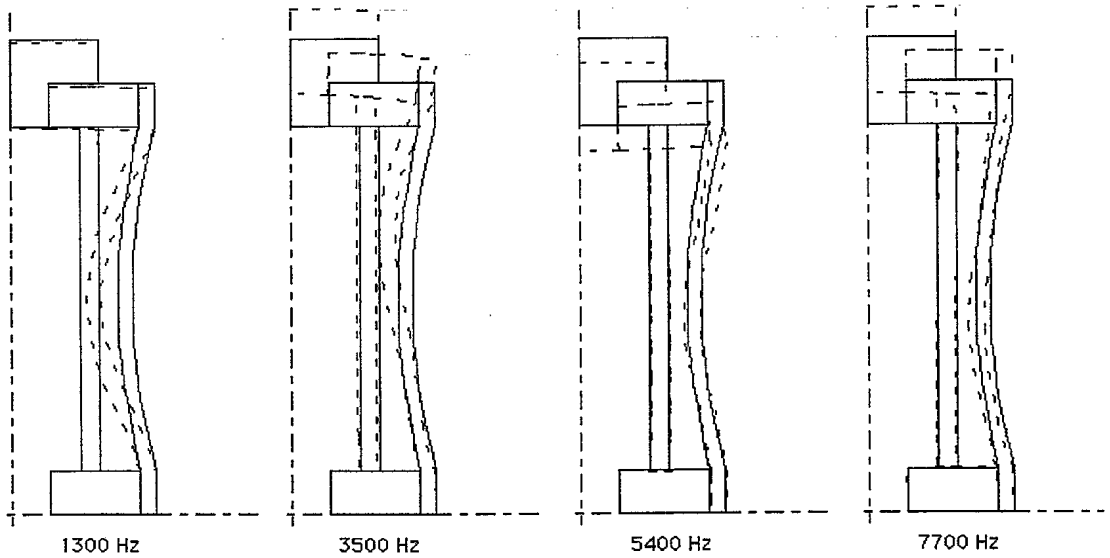

Figure 11 - Computed displacements at four drive frequencies corresponding approximately to the first and second stave resonances, the first longitudinal resonance, and a minimum in the TVR at 7700 Hz.

Computed and measured directivity patterns are compared in Figure 12 at two frequencies, 5.5 kHz and 9 kHz. The only other frequency at which directivity measurements were taken is 1.4 kHz, where both computed and measured patterns are essentially omnidirectional. The symmetry of the measured patterns showed an error in angle of 6°; this was corrected before using the data in Figure 12. Computed patterns at three other frequencies are shown in Figure 13. These correspond to the three upper frequencies of Figure 11.

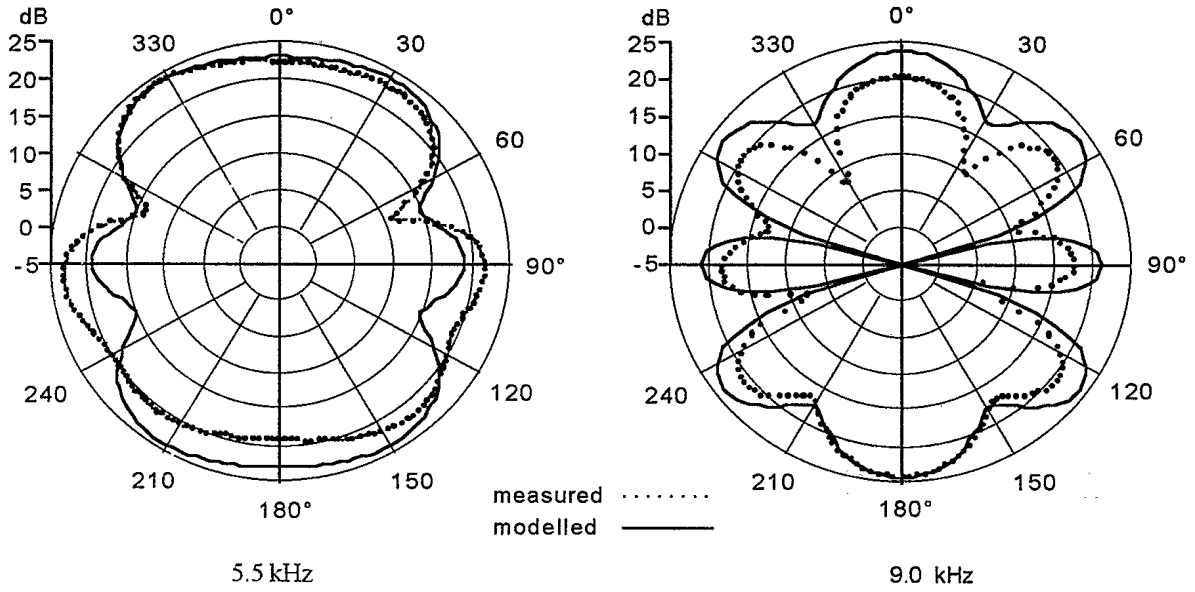

Figure 12 - Computed and measured XZ directivity patterns for the Class III BSP at 5.5 and 9 kHz. The radial scale is set arbitrarily and the maximum response for each curve is 24 dB.

6. Discussion

The fundamental flexural resonance frequency is about 130 Hz lower (i.e. 10% lower) than measured. The best explanation for this frequency difference is that the rubber boot has not been included in the model. It has been observed by Jones et al. [4] that the rubber boot stiffness significantly affects the fundamental flexural resonance frequency in water. For example, the measured difference in resonance frequency when a neoprene boot is replaced with a stiffer butyl boot on the Class III BSP in Ref. 4, is 80 Hz. Thus, it is believed that a better fit at the fundamental resonance can be obtained by including the rubber boot in the finite element model.

The 45% discrepancy in the value of the conductance at the fundamental flexural resonance may be due to experimental errors in the admittance measurements and the numerical errors associated with the approximations used in the 2D finite element model. It would be useful to obtain estimates for these errors in any follow-on work.

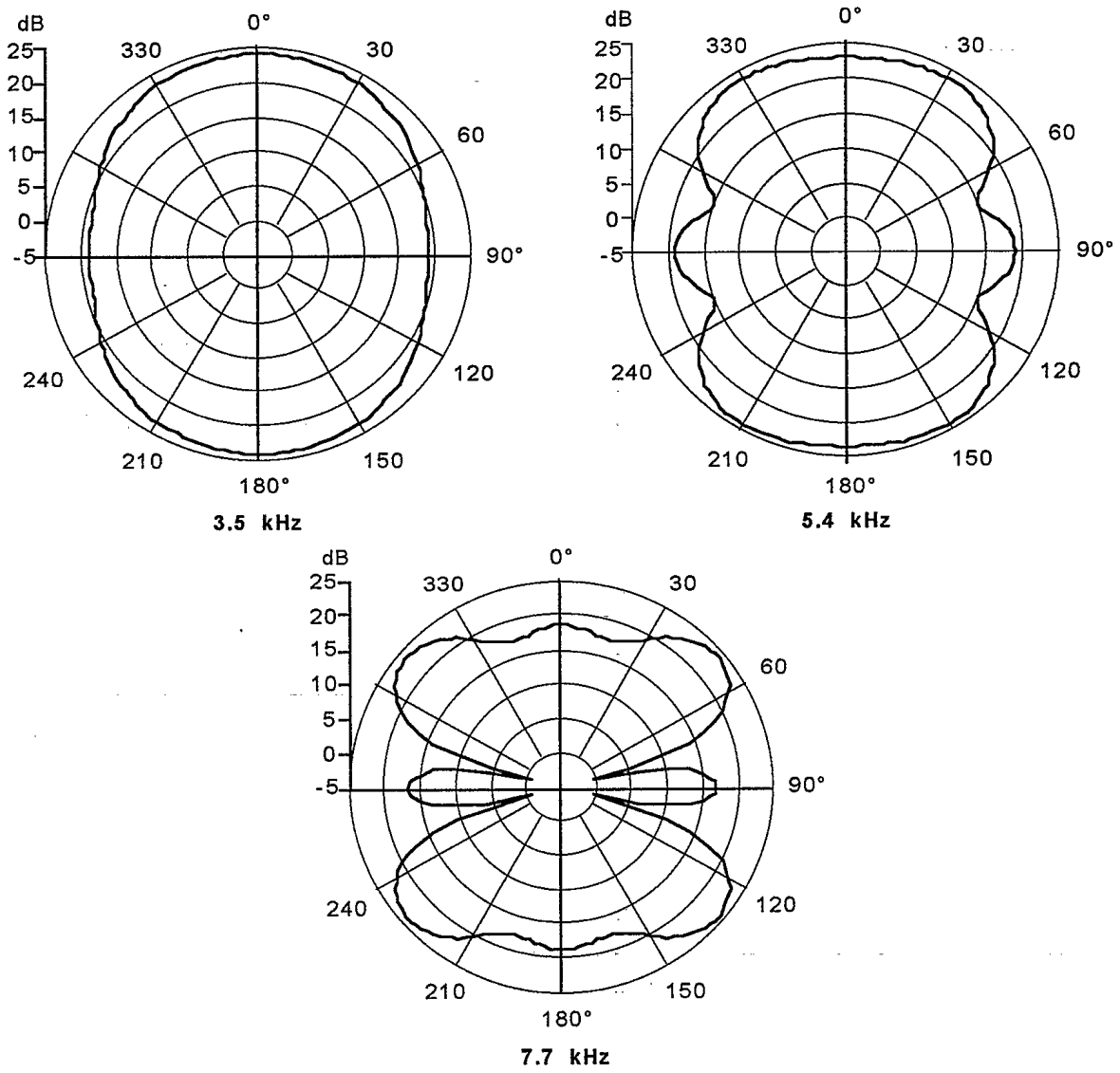

Figure 13 - Computed XZ directivity patterns for the Class III BSP at 3.5, 5.4, and 9 kHz. The radial scale is set arbitrarily and the maximum response for each curve is 24 dB.

Notwithstanding the above noted discrepancies, the model provides a good representation of the Class III BSP performance. The shape of the TVR curves and the directivity patterns conform well to the measured results. The directivity pattern lobe amplitudes agree to better than 4 dB and the angles of the lobes and nulls are in very close agreement.

The dip in TVR at 8 kHz may be due to misalignment of the transducer during the measurements. We note from the directivity pattern at 7.7 kHz in Figure 13, that a few degrees misalignment could cause a large dip in response.

The model does not predict the response between the two major resonances to be as high as measured. This is an important region when one is seeking useful power output over a broad band. Possibly a better prediction could be achieved by adjustment of the damping factors in the model, together with the inclusion of the neoprene boot in the model. It is expected that the boot causes most of the damping and this has been simulated by applying a high damping (10%) in the stave material. A damping factor of 5% is applied to the ceramic, which may be too high.

Note that the full sphere model (Fig. 2) is not perfectly symmetrical in the z=0 plane; the fluid elements adjacent to the upper end cap are cylindrical and can easily be changed to epoxy potting plastic to represent the electrical cable attachment if desired.

Only one example of stress contour plotting has been presented (Fig. 6), resulting from a static analysis. Dynamic stress contour plots from driven analyses can also be produced and any part of the structure can be expanded to display more detail. Stresses or strains can be plotted for any of the three coordinate directions, Z, R, and Ø.

Near-field pressure contours can be plotted in the sphere of fluid surrounding the transducer. This information might be useful in predicting the maximum available power level before the onset of cavitation.

References

[1] D.F. Jones and J.F. Lindberg, "Recent transduction developments in Canada and the United States," in Proc. I.O.A., Vol. 17, Pt. 3, 15-33 (1995).

[2] D.F. Jones and C.G. Reithmeier, "The acoustic performance of a Class III barrel-stave flextensional projector," in Proc. UDT, 103-108 (1996).

[3] D.F. Jones, "Research and Development of the 800 Hz Barrel-Stave Flextensional Transducer at the Defence Research Establishment Atlantic," DREA Report 98/101, January 1998.

[4] D.F. Jones, D.J. Lewis, C.G. Reithmeier, and G.A. Brownell, "Barrel-Stave Flextensional Transducers for Sonar Applications," DE-Vol. 84-2, 1995 Design Engineering Technical Conferences, Volume 3, Part B, ASME 1995, pp. 517-524.

UNCLASSIFIED
SECURITY CLASSIFICATION OF FORM
(highest classification of Title, Abstract, Keywords)

DOCUMENT CONTROL DATA

(Security classification of title, body of abstract and indexing annotation must be entered when the overall document is classified)

1. ORIGINATOR (the name and address of the organization preparing the document.. Organizations for whom the document was prepared, e.g. Establishment sponsoring a contractor's report, or tasking agency, are entered in section 8.)

FanTech Consulting Service
PO Box 503
Stewiacke, Nova Scotia B0N 2J0

2. SECURITY CLASSIFICATION (overall security classification of the document including special warning terms if applicable).

UNCLASSIFIED

3. TITLE (the complete document title as indicated on the title page. Its classification should be indicated by the appropriate abbreviation (S,C,R or U) in parentheses after the title).

Finite Element Analysis of a Broadband Flextensional Transducer

4. AUTHORS (Last name, first name, middle initial. If military, show rank, e.g. Doe, Maj. John E.)

G.W. McMahon

5. DATE OF PUBLICATION (month and year of publication of document)

January 1999

6a. NO .OF PAGES (total containing information Include Annexes, Appendices, etc).

19

6b. NO. OF REFS (total cited in document)

4

7. DESCRIPTIVE NOTES (the category of the document, e.g. technical report, technical note or memorandum. If appropriate, enter the type of report, e.g. interim, progress, summary, annual or final. Give the inclusive dates when a specific reporting period is covered).

CONTRACTOR REPORT

8. SPONSORING ACTIVITY (the name of the department project office or laboratory sponsoring the research and development. Include address).

Defence Research Establishment Atlantic
PO Box 1012
Dartmouth, NS, Canada B2Y 3Z7

9a. PROJECT OR GRANT NO. (if appropriate, the applicable research and development project or grant number under which the document was written. Please specify whether project or grant).

1cb11

9b. CONTRACT NO. (if appropriate, the applicable number under which the document was written).

W7707-8-5999/001/HAL

10a ORIGINATOR'S DOCUMENT NUMBER (the official document number by which the document is identified by the originating activity. This number must be unique to this document.)

10b OTHER DOCUMENT NOs. (Any other numbers which may be assigned this document either by the originator or by the sponsor.)

DREA CR 1999-008

11. DOCUMENT AVAILABILITY (any limitations on further dissemination of the document, other than those imposed by security classification)

(X) Unlimited distribution
( ) Defence departments and defence contractors; further distribution only as approved
( ) Defence departments and Canadian defence contractors; further distribution only as approved
( ) Government departments and agencies; further distribution only as approved
( ) Defence departments; further distribution only as approved
( ) Other (please specify):

12. DOCUMENT ANNOUNCEMENT (any limitation to the bibliographic announcement of this document. This will normally correspond to the Document Availability (11). However, where further distribution (beyond the audience specified in (11) is possible, a wider announcement audience may be selected).

No Limitation

UNCLASSIFIED
SECURITY CLASSIFICATION OF FORM

13. ABSTRACT (a brief and factual summary of the document. It may also appear elsewhere in the body of the document itself. It is highly desirable that the abstract of classified documents be unclassified. Each paragraph of the abstract shall begin with an indication of the security classification of the information in the paragraph (unless the document itself is unclassified) represented as (S), (C), (R), or (U). It is not necessary to include here abstracts in both official languages unless the text is bilingual).

The Class III flextensional transducer is a dual barrel stave design that shows promise as a broadband projector having a potentially useful bandwidth of over three octaves. A simple axially-symmetric finite element model, for use with the computer modelling program, MAVART, has been set up to aid in the optimization of this design. Performance results predicted by the model are compared with measured results for a DREA experimental Class III barrel-stave projector. The model provides a good representation of the performance, the main discrepancy being in the fundamental resonance frequency, which is 10 % lower than measured. The rubber boot, which was not included in the model, is believed to be the primary reason for the discrepancy. This model will be a useful tool for investigation of changes to the Class III BSP. Greater accuracy is expected with the inclusion of the rubber boot in the model.

14. KEYWORDS, DESCRIPTORS or IDENTIFIERS (technically meaningful terms or short phrases that characterize a document and could be helpful in cataloguing the document. They should be selected so that no security classification is required. Identifiers, such as equipment model designation, trade name, military project code name, geographic location may also be included. If possible keywords should be selected from a published thesaurus. e.g. Thesaurus of Engineering and Scientific Terms (TEST) and that thesaurus-identified. If it not possible to select indexing terms which are Unclassified, the classification of each should be indicated as with the title).

Sonar transducer
Piezoelectric transducer
Broadband transducer
Flextensional transducer
Finite element analysis

Leader en sciences et
technologie de la défense,
la Direction de la recherche
et du développement pour
la défense contribue
à maintenir et à
accroître les compétences
du Canada dans
ce domaine.

The Defence Research
and Development Branch
provides Science and
Technology leadership
in the advancement and
maintenance of Canada's
defence capabilities.

DEFENCE R&D DÉFENSE

www.crad.dnd.ca